Letter

Kagome chiral spin liquid in transition metal dichalcogenide moiré bilayers

Johannes Motruk,[1,*] Dario Rossi,[1] Dmitry A. Abanin,[1,2] and Louk Rademaker[1,3]
[1]*Department of Theoretical Physics, University of Geneva, Quai Ernest-Ansermet 24, 1205 Geneva, Switzerland*
[2]*Google Research, Mountain View, California, USA*
[3]*Department of Quantum Matter Physics, University of Geneva, Quai Ernest-Ansermet 24, 1205 Geneva, Switzerland*

(Received 5 December 2022; revised 27 April 2023; accepted 2 May 2023; published 5 June 2023)

At $n = 3/4$ filling of the moiré flat band, transition metal dichalcogenide (TMD) moiré bilayers will develop kagome charge order. We derive an effective spin model for the resulting localized spins and find that its further neighbor spin interactions can be much less suppressed than the corresponding electron hopping strength. Using density matrix renormalization group simulations, we study its phase diagram and, for realistic model parameters relevant for WSe_2/WS_2, we show that this material can realize the exotic chiral spin liquid phase and the highly debated kagome spin liquid. Our work thus demonstrates that the frustration and strong interactions present in TMD heterobilayers provide an exciting platform to study spin liquid physics.

DOI: 10.1103/PhysRevResearch.5.L022049

Introduction. The recent surge in moiré materials has vastly expanded the number of experimental platforms with strongly correlated electrons. While this was jump-started by the discovery of correlated insulating states and superconductivity in twisted bilayer graphene [1–4], the strength of electron correlations in bilayers of transition metal dichalcogenide (TMD) materials exceeds those in their graphene cousins [5]. Experiments in TMDs have revealed signatures of Mott insulators [6–10], the quantum anomalous Hall effect [11], and—in heterobilayers—generalized Mott-Wigner crystals at fractional fillings [7,12–16]. When the electron charges are localized, only the spin degree of freedom remains, and magnetism in TMD moiré bilayers started to be investigated in recent experiments [17–19]. Heterobilayers realize an extended Hubbard model on the triangular lattice [20–23], and consequently the localized spins are highly frustrated. This frustration might lead to a spin liquid phase, an exotic state of matter whose material realization is long sought for [24,25].

In this Letter, we show that the generalized Mott-Wigner states at $n = \pm 3/4$ filling, reported for WSe_2/WS_2 bilayers [12,13], can realize both a *chiral spin liquid* [26,27] and the *kagome spin liquid* (KSL) [28–33]. At this particular filling, electrons are localized on an effective kagome lattice, which is known for its high degree of geometrical frustration. Here, we demonstrate how realistic model parameters lead to an effective spin model on this kagome lattice and investigate the model using extensive state-of-the-art density matrix renormalization group (DMRG) simulations [34,35]. The tunability of TMD bilayers—changing twist angle, gate tuning, material and dielectric environment choice, pressure, and so forth—thus allows for a systematic pursuit of spin liquid phases [36–39].

Model. The moiré pattern of TMD heterobilayers is formed due to the lattice mismatch between the two layers, where the effective moiré length can be tuned by adjusting the twist angle. The interlayer band alignment ensures that the first conduction or valence flat band is completely localized in one of the layers. Based on our earlier work [22], we describe the resulting flat bands by a spin-orbit-coupled extended Hubbard model on the triangular lattice,

$$H = \sum_{jk,\sigma} |t_{jk}| e^{-i\sigma\phi_{jk}} c^\dagger_{j\sigma} c_{k\sigma} + \text{H.c.} + U \sum_j n_{j\uparrow} n_{j\downarrow} + V \sum_{\langle jk\rangle,\sigma} n_{j\sigma} n_{k\sigma}, \quad (1)$$

where $\langle jk\rangle$ denotes nearest-neighbor sites. We include the hopping matrix elements t_{jk} up to third-nearest neighbor, where ϕ_{jk} represent their phases induced by spin-orbit coupling.

When the nearest-neighbor repulsion is sufficiently large, a charge density wave is stabilized at commensurate fillings. In particular, at $n = \pm 3/4$ filling, the charge order forms a kagome lattice, as shown in Fig. 1(c) [40,41]. In the Supplemental Material (SM) [42–44], we show, using a simple mean-field theory, that the charges are almost completely localized on the kagome lattice when $V/t_1 \geqslant 5$. To study the spin degree of freedom of these localized charges, we derive an effective spin model on the kagome lattice, starting from the extended Hubbard model of Eq. (1) [45,46]. In our strong-coupling expansion, we keep all terms of second and third order in the hoppings, and up to fourth-order contributions proportional to the nearest-neighbor hopping t_1. We employ the method introduced in Ref. [47] and the derivation and coefficients of the model are provided in detail in the SM [42].

*johannes.motruk@unige.ch

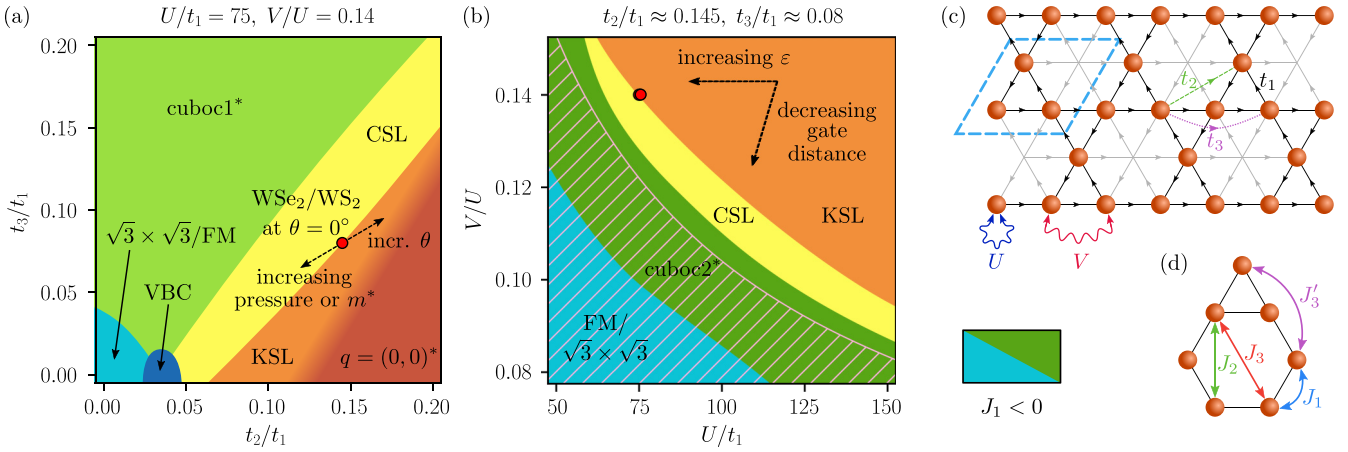

FIG. 1. (a) Ground-state phase diagram of the effective spin model (2) for $U/t_1 = 75$ and $V/t_1 = 10.5$—corresponding to the interactions for $\varepsilon \approx 9.5$ in WSe_2/WS_2 at $\theta = 0°$—as a function of t_2/t_1 and t_3/t_1. The phases appearing are the chiral spin liquid (CSL), the kagome spin liquid (KSL) connected to the ground state of the nearest-neighbor Heisenberg Hamiltonian, a valence bond crystal (VBC), and cuboc1*, $q = (0,0)^*$, and $\sqrt{3}\times\sqrt{3}$ or ferromagnetically ordered phases. The $\sqrt{3}\times\sqrt{3}$ and ferromagnet are energetically degenerate. The red dot indicates the t_2/t_1 and t_3/t_1 values for WSe_2/WS_2 at $\theta = 0°$. Arrows show how this point would shift qualitatively when tuning twist angle, pressure or changing the effective mass by a different material choice. (b) Phase diagram for $t_2/t_1 \approx 0.145$ and $t_3/t_1 \approx 0.08$—corresponding to WSe_2/WS_2 at $\theta = 0°$—as a function of U/t_1 and V/U. Here, the cuboc2* phase emerges as an additional magnetically ordered phase. The ratio of V/U can be tuned by the gate distance while U/t_1 changes with different dielectric environment. Crucially, the system can be tuned into the CSL by merely changing the gate distance across almost the entire range of interaction strength. The hatched area denotes the region in which J_1 is negative (ferromagnetic) and the red dot indicates the interaction values of panel (a). The data underlying the phase diagrams have been obtained on an infinite YC8 cylinder. (c) Extended Hubbard model at 3/4 filling with all charges localized on a kagome lattice. The unit cell of the charge ordering is indicated by the blue-lined box. When a spin-↑ particle hops from a site j to a site k along the direction of an arrow, it picks up a phase of ϕ_{jk}. (d) Interactions of the resulting spin model on the kagome lattice.

The resulting spin model is given by

$$H_{\text{spin}} = \sum_{ij} J_{ij}\big[S_i^z S_j^z + \cos(\tilde{\phi}_{ij})\big(S_i^x S_j^x + S_i^y S_j^y\big) + \sin(\tilde{\phi}_{ij})(\boldsymbol{S}_i \times \boldsymbol{S}_j)\cdot\hat{\mathbf{z}}\big], \tag{2}$$

where the $\tilde{\phi}_{ij}$ are linear combinations of the ϕ_{jk} phases from Eq. (1), and we neglected very small four-spin terms. The sum over ij runs over neighbors as illustrated in Fig. 1(d). The spin model of Eq. (2) contains XXZ and Dzyaloshinskii-Moriya (DM) terms caused by the nonzero phases ϕ_{jk} in the extended Hubbard model. These phases are constrained by symmetry [22] and translate into the phases for the spin model as follows: $\tilde{\phi}_1 = 4\pi/3$, $\tilde{\phi}_2 = 0$, and $\tilde{\phi}_3 = 2\pi/3$ for nearest, next-nearest, and next-next-nearest neighbor couplings, respectively. This combination allows for a local three sublattice gauge transformation (a spin rotation in the x-y plane) [42] that brings the model into SU(2)-invariant form, hence, the model still exhibits a hidden SU(2) symmetry [48–50]. As a result, the *structure* of the phase diagram of our kagome spin model (2) coincides exactly with that of an SU(2)-invariant J_1-J_2-J_3-J_3' model on the kagome lattice, despite the presence of the DM interactions. The phase diagram of this model for $J_3' = 0$ has been studied previously with DMRG [51]. We remark here already that the numerical results we report are consistent with this previous work in the range of parameters studied in Ref. [51]. Note, however, that the spin patterns in the magnetically ordered phases are changed by the gauge transformation relative to the phases of the SU(2)-invariant model.

Before presenting the numerical results, let us analyze how the spin model coefficients emerge from realistic material parameters. In Fig. 2, we show the contributions of the different orders of the expansion to J_1, J_2, and J_3 for WSe_2/WS_2. It is evident that the third and fourth orders are extremely important to capture the correct physics. Being ferromagnetic for J_1, the third and fourth orders suppress J_1 turning it even negative for larger twist angles (smaller interactions). In the case of J_2 and J_3, on the other hand, the spin interactions are boosted by the higher orders. In this way, J_1, J_2, and J_3 can be of the same order of magnitude permitting the rich phase diagrams tunable with experimental parameters we report below, despite t_2 and t_3 being an order of magnitude smaller than t_1. Note that this is not a sign of a breakdown of our expansion, but rather

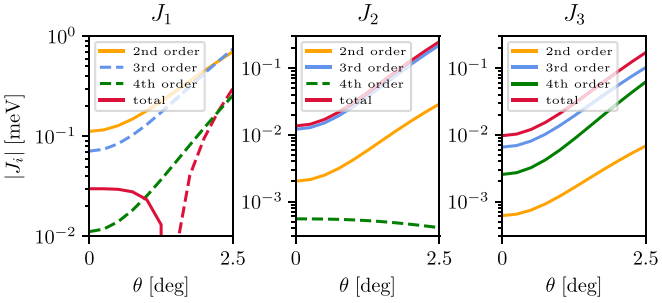

FIG. 2. Contributions of the different orders of the effective Hamiltonian from our DFT estimates for WSe_2/WS_2 and dielectric screening with $\varepsilon = 9.5$ as a function of twist angle. Dashed lines denote negative values.

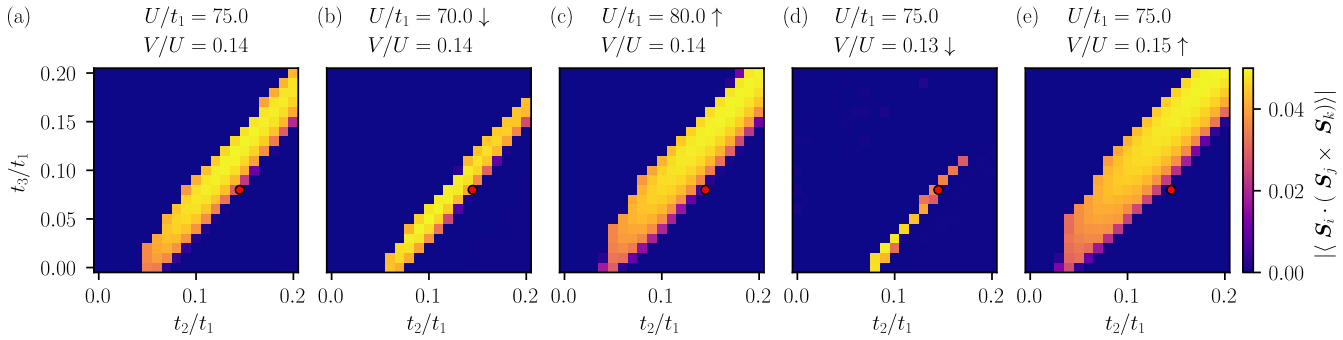

FIG. 3. CSL region as a function of t_2/t_1 and t_3/t_1 for various combinations of U and V from DMRG on an infinite YC8 cylinder as detected by the absolute value of the chiral order parameter $\langle \boldsymbol{S}_i \cdot (\boldsymbol{S}_j \times \boldsymbol{S}_k) \rangle$ averaged over all small nearest-neighbor triangles on the kagome lattice. (a) $U/t_1 = 75$ and $V/U = 0.14$ corresponding to the phase diagram in Fig. 1(a). (b) For decreased $U/t_1 = 70$ with $V/U = 0.14$ unchanged, the CSL region moves slightly to the lower right, but narrows. (c) Opposite effect when increasing to $U/t_1 = 70$, still at $V/U = 0.14$. (d) Changing $V/U = 0.13$ has a similar effect as decreasing U, (e) larger $V/U = 0.15$ behaves comparable to increased U.

comes from the fact that the higher orders include virtual processes that do not involve intermediate states with a double occupancy and whose contribution is therefore not suppressed by factors of $1/U$.

Numerical results. To obtain the ground-state phase diagram of our spin model, we perform DMRG simulations on an infinite cylinder of YC8 geometry [29,42]. We map out the phase diagram for fixed $U/t_1 = 75$ and $V/U = 0.14$ for varying t_2/t_1 and t_3/t_1, and for fixed $t_2/t_1 \approx 0.145$ and $t_3/t_1 \approx 0.08$ for varying U/t_1 and V/U, shown in Figs. 1(a) and 1(b), respectively. The interaction strengths of Fig. 1(a) correspond to the estimates for WSe_2/WS_2 at $\theta = 0^\circ$ twist angle with dielectric constant $\varepsilon \approx 9.5$. The same holds for the t ratios of Fig. 1(b). The derivation of these model parameters from *ab initio* calculations is detailed in our SM [42]. For fixed interactions in Fig. 1(a), we find two spin liquid phases, namely the CSL [51–55] and the KSL, which is connected to the nearest-neighbor Heisenberg point. For small t_2 and t_3, we observe a phase in which a ferromagnet and a $\sqrt{3} \times \sqrt{3}$ state [56–58] in the x-y plane are the degenerate ground states due to the gauge transformation [42]. In an SU(2)-invariant version of the model, these would be the two degenerate $\sqrt{3} \times \sqrt{3}$ states with opposite vector chirality. Next to it, we find a valence bond crystal (VBC) with spontaneous bond order. Above the diagonal, the phase diagram is dominated by the cuboc1* state, the gauge transformed version of the cuboc1 state, a state with finite scalar chirality [59]. On the bottom right, the ground state is the $q = (0, 0)^*$ state, the gauge transformed version of the coplanar $q = (0, 0)$ order [56,58,60]. The relation between the magnetic orders, the gauge transformation and the states of the SU(2)-invariant Hamiltonian is further discussed in the SM [42].

The phase diagram in Fig. 1(b), with the hopping values fixed at our estimates for WSe_2/WS_2 at $\theta = 0^\circ$ similarly exhibits a finite CSL region in the center. For stronger interactions, the KSL takes over. For smaller U and V, we find the cuboc2* state, the gauge transformed version of the cuboc2 magnetic order [59], and again a region with degenerate ferromagnetic and $\sqrt{3} \times \sqrt{3}$ ground states. Most of these two phases coincide with the area in which the nearest-neighbor spin interaction turns ferromagnetic, in agreement with classical phase diagrams [59].

Chiral spin liquid. To identify the CSL, we primarily use the chiral order parameter (OP) $\langle \boldsymbol{S}_i \cdot (\boldsymbol{S}_j \times \boldsymbol{S}_k) \rangle$ where i, j, and k denote the sites around a small triangle in the kagome lattice formed out of nearest-neighbor bonds. The chiral OP for the various values of U and V is depicted in Fig. 3 and clearly indicates the region of the CSL. We observe that the CSL region widens or narrows and shifts with changing interactions. We note that both the cuboc1* phase as well as the $q = (0, 0)^*$ phase can attain a nonzero chirality on the small triangles, but in a staggered pattern such that it averages out over the unit cell.

Since the chiral OP alone is not an unambiguous signature of the CSL, we also compute the momentum-resolved entanglement spectrum and the spin Hall conductivity from flux insertion. In the entanglement spectrum, a momentum k_y around the cylinder and S^z eigenvalue of the corresponding Schmidt state can be assigned to each level. The chiral $SU(2)_1$ Wess-Zumino-Witten (WZW) conformal field theory describing the edge of the CSL then predicts a certain multiplet structure in each S^z sector [61–63], which we confirm in Fig. 4(a). We show the response of the system when threading spin flux through the cylinder in Fig. 4(b). We

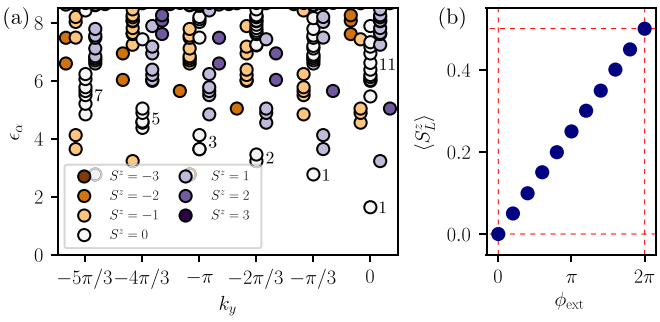

FIG. 4. (a) Momentum-resolved entanglement spectrum in the CSL phase on a YC12 cylinder. The S^z sectors of the levels show the counting pattern expected from the CFT describing the edge states $(1, 1, 2, 3, 5, 7, \ldots)$. (b) Expectation value $\langle S^z_L \rangle$ value of the left half of the cylinder under spin flux insertion. $\Delta\langle S^z \rangle = 1/2$ is pumped from the right to the left half of the cylinder under 2π flux insertion indicating a spin Hall conductivity of $\sigma^{\text{spin}}_{xy} = 1/2$.

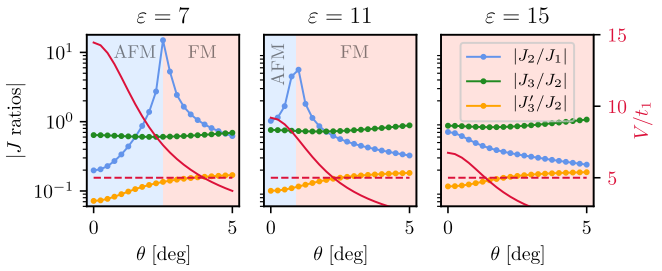

FIG. 5. Absolute values of J ratios from our DFT estimates for WSe_2/WS_2 as a function of twist angle for different values of ε. For $\varepsilon = 7$ and 11, the ratio J_2/J_1 changes sign due to J_1 becoming negative indicated by the blue (positive) and red (negative) shading. At $\varepsilon = 15$, J_1 is negative over the entire twist angle range. J_2 and J_3 are positive everywhere while J_3' is always negative. We chose the absolute values here for better presentation clarity on a log scale. We also include the ratio of V/t_1 (red line) and $V/t_1 = 5$ (red dashed line). Above this value, almost the entire particle density is localized on the kagome lattice, ensuring the validity of our spin model description.

replace each term $S_j^+ S_k^- \to S_j^+ S_k^- e^{i\phi_{\rm ext}(y_j - y_k)/L_y}$, so that a spin up picks up a phase of $e^{i\phi_{\rm ext}}$ when going around the circumference. After $\phi_{\rm ext} = 2\pi$ flux insertion, the expectation value of the spin in the left half of the system increases by $\langle S^z \rangle = 1/2$, which implies a quantized spin Hall conductivity of $\sigma_{xy}^{\rm spin} = 1/2$, as expected for the Kalmeyer-Laughlin CSL [26].

Kagome spin liquid. The presumed ground state of the kagome spin model with only nearest-neighbor Heisenberg coupling is also a spin liquid, whose nature remains under debate [28–33,64–69]. In our t_2-t_3 phase diagram in Fig. 1(a), we find a small strip of the KSL below the CSL. However, the separation between the KSL the $q = (0, 0)^*$ state is subtle to detect. The spins in the $q = (0, 0)^*$ can partly point out of the x-y plane which happens in the region of the phase diagram that we ascribe to the $q = (0, 0)^*$ phase. The part that we identify as the KSL has $\langle S_i^z \rangle = 0$. The latter region could also be a weakly ordered $q = (0, 0)^*$ state with spins lying in the x-y plane. However, at negative $t_3/t_1 \approx -0.032$ and $t_2/t_1 \approx 0.04$, J_2 and J_3 almost vanish and we obtain a nearly-only nearest-neighbor spin model. Since we find no signs of a quantum phase transition between this point and the $\langle S_i^z \rangle = 0$ region in question, we assign it to the KSL phase and take the line at which a finite $\langle S_i^z \rangle$ develops as the phase boundary. The details of this reasoning are given in the SM [42]. We emphasize that it is not within the scope of this work to give further insight into the nature of the KSL phase, but that we identify a phase with paramagnetic features which is distinct from the $q = (0, 0)^*$ phase and adiabatically connected to the ground state of the nearest-neighbor-only model. By this identification of phases, the entire upper right region in the V-U phase diagram of Fig. 1(b) falls into the KSL phase as well.

Experimental realization and detection. The red dots in our phase diagrams in Fig. 1 mark our estimate for the hopping and interaction values at $\varepsilon \approx 9.5$ for the first flat valence band in aligned WSe_2/WS_2 [22,42]. We thus predict that aligned WSe_2/WS_2 falls just onto the transition line between the CSL and the KSL, suggesting a real material manifestation of these exotic spin states. As in any TMD heterobilayer, the interaction strengths U/t_i and V/t_i are tunable through engineering the dielectric environment. The ratio V/U can be changed by adjusting the screening length, which can be modified by the distance between the conducting gates and the bilayer. The influence of these two tuning knobs is demonstrated in Fig. 1(b), which shows that the system can be driven deeper into one of the spin liquid phases. In addition to the dielectric environment and gate distance, there are several other tuning parameters. The choice of TMD material influences the effective model—most notably, compounds with Mo have a larger particle effective mass than We-based TMDs, which then leads to flatter bands and larger effective interactions U/t_i, V/t_i. Similarly, applying uniaxial pressure onto the bilayer increases the interlayer moiré potential, which strengthens interactions as well. We found that these two factors also lead to a slight increase in the t_3/t_2 ratio. On the other hand, the interaction strength can be reduced by increasing the twist angle.

The values of the resulting spin interactions in WSe_2/WS_2 as a function of twist angle for different values of ε are shown in Fig. 5. Generally, the magnitudes of the coefficients are distributed as expected with $|J_1| > |J_2| > |J_3| > |J_3'|$. As discussed above, J_1 turns negative and we obtain a ferromagnetic model for larger ε and/or twist angle while J_2 and J_3 always stay positive and J_3' negative. The relevant energy scale for the spin physics we consider is given by the nearest-neighbor exchange constant J_1 which is rather small due the large length scale in moiré systems. For the value of $U/t_1 = 75$ in Fig. 1(a), our estimates lead to $J_1 \approx 0.03$ meV corresponding to ≈350 mK which severely challenges experimental detection of the exotic spin phases. It has been proposed that magnetic order can be diagnosed by the splitting of exciton resonances [70]. Further promising techniques include magnetic resonance force microscopy (MRFM) [71], spin-polarized scanning tunnel microscopy (STM) [72], and nitrogen vacancy (NV) centers [73]. The detection of spin liquids beyond the absence of magnetic order is even more challenging. One possible approach is to use the optical access to the spin degree of freedom in TMDs due to spin-valley locking [74,75] which may allow for the dynamical detection of the time-reversal symmetry breaking or quantized spin Hall conductivity of the CSL. Recently, magneto-optical Faraday rotation was proposed to detect the CSL in the triangular lattice Hubbard model [37,76].

Conclusion. We have demonstrated that a variety of magnetic phases can be realized in an effective spin model on the kagome lattice which describes TMD bilayers at a filling of 3/4 holes or electrons. In particular, the chiral spin liquid as well as the kagome spin liquid can emerge for experimentally realistic parameters, in addition to several magnetically ordered phases. Moreover, the tunability of TMD moiré systems allows for a systematic search of elusive spin liquid physics, and as such it opens up a promising new direction in the search of highly entangled quantum matter. Apart from our approach, two additional proposals for a kagome charge arrangement in twisted TMD bilayers have recently been put forward whose spin physics has yet to be investigated [77,78].

The data and code used to create the reported results are available at [79].

Acknowledgments. Support by the Swiss National Science Foundation (SNSF) under Grant No. 188532 and by the European Research Council (ERC) under the European Union's Horizon 2020 research and innovation programme (Grant Agreement No. 864597) is gratefully acknowledged. J.M. was supported by the SNSF Swiss Postdoctoral Fellowship grant 210478. L.R. was funded by the SNSF via Ambizione Grant 174208 and SNSF Starting Grant 211296. DMRG simulations were performed using the TeNPy library [80] on the Baobab and Yggdrasil HPC clusters at the University of Geneva.

[1] Y. Cao, V. Fatemi, S. Fang, K. Watanabe, T. Taniguchi, E. Kaxiras, and P. Jarillo-Herrero, Unconventional superconductivity in magic-angle graphene superlattices, Nature (London) **556**, 43 (2018).

[2] Y. Cao, V. Fatemi, A. Demir, S. Fang, S. L. Tomarken, J. Y. Luo, J. D. Sanchez-Yamagishi, K. Watanabe, T. Taniguchi, E. Kaxiras, R. C. Ashoori, and P. Jarillo-Herrero, Correlated insulator behaviour at half-filling in magic-angle graphene superlattices, Nature (London) **556**, 80 (2018).

[3] L. Balents, C. R. Dean, D. K. Efetov, and A. F. Young, Superconductivity and strong correlations in moiré flat bands, Nat. Phys. **16**, 725 (2020).

[4] E. Y. Andrei and A. H. MacDonald, Graphene bilayers with a twist, Nat. Mater. **19**, 1265 (2020).

[5] K. F. Mak and J. Shan, Semiconductor moiré materials, Nat. Nanotechnol. **17**, 686 (2022).

[6] Y. Tang, L. Li, T. Li, Y. Xu, S. Liu, K. Barmak, K. Watanabe, T. Taniguchi, A. H. MacDonald, J. Shan, and K. F. Mak, Simulation of Hubbard model physics in WSe_2/WS_2 moiré superlattices, Nature (London) **579**, 353 (2020).

[7] E. C. Regan, D. Wang, C. Jin, M. I. B. Utama, B. Gao, X. Wei, S. Zhao, W. Zhao, Z. Zhang, K. Yumigeta, M. Blei, J. D. Carlström, K. Watanabe, T. Taniguchi, S. Tongay, M. Crommie, A. Zettl, and F. Wang, Mott and generalized Wigner crystal states in WSe_2/WS_2 moiré superlattices, Nature (London) **579**, 359 (2020).

[8] L. Wang, E.-M. Shih, A. Ghiotto, L. Xian, D. A. Rhodes, C. Tan, M. Claassen, D. M. Kennes, Y. Bai, B. Kim, K. Watanabe, T. Taniguchi, X. Zhu, J. Hone, A. Rubio, A. N. Pasupathy, and C. R. Dean, Correlated electronic phases in twisted bilayer transition metal dichalcogenides, Nat. Mater. **19**, 1 (2020).

[9] T. Li, S. Jiang, L. Li, Y. Zhang, K. Kang, J. Zhu, K. Watanabe, T. Taniguchi, D. Chowdhury, L. Fu, J. Shan, and K. F. Mak, Continuous Mott transition in semiconductor moiré superlattices, Nature (London) **597**, 350 (2021).

[10] A. Ghiotto, E.-M. Shih, G. S. S. G. Pereira, D. A. Rhodes, B. Kim, J. Zang, A. J. Millis, K. Watanabe, T. Taniguchi, J. C. Hone, L. Wang, C. R. Dean, and A. N. Pasupathy, Quantum criticality in twisted transition metal dichalcogenides, Nature (London) **597**, 345 (2021).

[11] T. Li, S. Jiang, B. Shen, Y. Zhang, L. Li, Z. Tao, T. Devakul, K. Watanabe, T. Taniguchi, L. Fu, J. Shan, and K. F. Mak, Quantum anomalous Hall effect from intertwined moiré bands, Nature (London) **600**, 641 (2021).

[12] Y. Xu, S. Liu, D. A. Rhodes, K. Watanabe, T. Taniguchi, J. Hone, V. Elser, K. F. Mak, and J. Shan, Correlated insulating states at fractional fillings of moiré superlattices, Nature (London) **587**, 214 (2020).

[13] X. Huang, T. Wang, S. Miao, C. Wang, Z. Li, Z. Lian, T. Taniguchi, K. Watanabe, S. Okamoto, D. Xiao, S.-F. Shi, and Y.-T. Cui, Correlated insulating states at fractional fillings of the WS_2/WSe_2 moiré lattice, Nat. Phys. **17**, 715 (2021).

[14] H. Li, S. Li, E. C. Regan, D. Wang, W. Zhao, S. Kahn, K. Yumigeta, M. Blei, T. Taniguchi, K. Watanabe, S. Tongay, A. Zettl, M. F. Crommie, and F. Wang, Imaging two-dimensional generalized Wigner crystals, Nature (London) **597**, 650 (2021).

[15] E. Liu, T. Taniguchi, K. Watanabe, N. M. Gabor, Y.-T. Cui, and C. H. Lui, Excitonic and Valley-Polarization Signatures of Fractional Correlated Electronic Phases in a WSe_2/WS_2 Moiré Superlattice, Phys. Rev. Lett. **127**, 037402 (2021).

[16] S. Miao, T. Wang, X. Huang, D. Chen, Z. Lian, C. Wang, M. Blei, T. Taniguchi, K. Watanabe, S. Tongay, Z. Wang, D. Xiao, Y.-T. Cui, and S.-F. Shi, Strong interaction between interlayer excitons and correlated electrons in WSe_2/WS_2 moiré superlattice, Nat. Commun. **12**, 3608 (2021).

[17] X. Wang, C. Xiao, H. Park, J. Zhu, C. Wang, T. Taniguchi, K. Watanabe, J. Yan, D. Xiao, D. R. Gamelin, W. Yao, and X. Xu, Light-induced ferromagnetism in moiré superlattices, Nature (London) **604**, 468 (2022).

[18] Y. Tang, K. Su, L. Li, Y. Xu, S. Liu, K. Watanabe, T. Taniguchi, J. Hone, C.-M. Jian, C. Xu, K. F. Mak, and J. Shan, Evidence of frustrated magnetic interactions in a Wigner–Mott insulator, Nat. Nanotechnol. **18**, 233 (2023).

[19] E. Anderson, F.-R. Fan, J. Cai, W. Holtzmann, T. Taniguchi, K. Watanabe, D. Xiao, W. Yao, and X. Xu, Programming correlated magnetic states via gate controlled moiré geometry, arXiv:2303.17038.

[20] F. Wu, T. Lovorn, E. Tutuc, and A. H. MacDonald, Hubbard Model Physics in Transition Metal Dichalcogenide Moiré Bands, Phys. Rev. Lett. **121**, 026402 (2018).

[21] Y. Zhang, N. F. Q. Yuan, and L. Fu, Moiré quantum chemistry: Charge transfer in transition metal dichalcogenide superlattices, Phys. Rev. B **102**, 201115(R) (2020).

[22] L. Rademaker, Spin-orbit coupling in transition metal dichalcogenide heterobilayer flat bands, Phys. Rev. B **105**, 195428 (2022).

[23] Y. Zhang, T. Devakul, and L. Fu, Spin-textured Chern bands in AB-stacked transition metal dichalcogenide bilayers, Proc. Natl. Acad. Sci. USA **118**, e2112673118 (2021).

[24] L. Savary and L. Balents, Quantum spin liquids: A review, Rep. Prog. Phys. **80**, 016502 (2016).

[25] J. Knolle and R. Moessner, A field guide to spin liquids, Annu. Rev. Condens. Matter Phys. **10**, 451 (2019).

[26] V. Kalmeyer and R. B. Laughlin, Equivalence of the Resonating-Valence-Bond and Fractional Quantum Hall States, Phys. Rev. Lett. **59**, 2095 (1987).

[27] D. F. Schroeter, E. Kapit, R. Thomale, and M. Greiter, Spin Hamiltonian for which the Chiral Spin Liquid is the Exact Ground State, Phys. Rev. Lett. **99**, 097202 (2007).

[28] H. C. Jiang, Z. Y. Weng, and D. N. Sheng, Density Matrix Renormalization Group Numerical Study of the Kagome Antiferromagnet, Phys. Rev. Lett. **101**, 117203 (2008).

[29] S. Yan, D. A. Huse, and S. R. White, Spin-liquid ground state of the $S = 1/2$ kagome Heisenberg antiferromagnet, Science **332**, 1173 (2011).

[30] H. J. Liao, Z. Y. Xie, J. Chen, Z. Y. Liu, H. D. Xie, R. Z. Huang, B. Normand, and T. Xiang, Gapless Spin-Liquid Ground State in the $S = 1/2$ Kagome Antiferromagnet, Phys. Rev. Lett. **118**, 137202 (2017).

[31] Y.-C. He, M. P. Zaletel, M. Oshikawa, and F. Pollmann, Signatures of Dirac Cones in a DMRG Study of the Kagome Heisenberg Model, Phys. Rev. X **7**, 031020 (2017).

[32] A. M. Läuchli, J. Sudan, and R. Moessner, $S = \frac{1}{2}$ kagome Heisenberg antiferromagnet revisited, Phys. Rev. B **100**, 155142 (2019).

[33] Y. Iqbal, F. Ferrari, A. Chauhan, A. Parola, D. Poilblanc, and F. Becca, Gutzwiller projected states for the $J_1 - J_2$ Heisenberg model on the Kagome lattice: Achievements and pitfalls, Phys. Rev. B **104**, 144406 (2021).

[34] S. R. White, Density Matrix Formulation for Quantum Renormalization Groups, Phys. Rev. Lett. **69**, 2863 (1992).

[35] I. P. McCulloch, Infinite size density matrix renormalization group, revisited, arXiv:0804.2509.

[36] Y. Zhou, D. N. Sheng, and E.-A. Kim, Quantum Phases of Transition Metal Dichalcogenide Moiré Systems, Phys. Rev. Lett. **128**, 157602 (2022).

[37] A. Szasz, J. Motruk, M. P. Zaletel, and J. E. Moore, Chiral Spin Liquid Phase of the Triangular Lattice Hubbard Model: A Density Matrix Renormalization Group Study, Phys. Rev. X **10**, 021042 (2020).

[38] D. Kiese, Y. He, C. Hickey, A. Rubio, and D. M. Kennes, TMDs as a platform for spin liquid physics: A strong coupling study of twisted bilayer WSe_2, APL Mater. **10**, 031113 (2022).

[39] C. Kuhlenkamp, W. Kadow, A. İmamoğlu, and M. Knap, Tunable topological order of pseudo spins in semiconductor heterostructures, arXiv:2209.05506.

[40] H. Pan, F. Wu, and S. Das Sarma, Quantum phase diagram of a moiré-Hubbard model, Phys. Rev. B **102**, 201104(R) (2020).

[41] Y. Tan, P. K. H. Tsang, V. Dobrosavljević, and L. Rademaker, Doping a Wigner-Mott insulator: Electron slush in transition-metal dichalcogenide moiré heterobilayers, arXiv:2210.07926.

[42] See Supplemental Material at http://link.aps.org/supplemental/10.1103/PhysRevResearch.5.L022049 for details on the *ab initio* calculations of the model parameters, mean-field theory of the charge order, derivation of the effective spin model, DMRG parameters, nature of the gauge transformation, characterization of magnetic states, and distinguishing the KSL from the $q = (0, 0)^*$ order, which includes Refs. [42,43].

[43] A. H. MacDonald, S. M. Girvin, and D. Yoshioka, $\frac{t}{U}$ expansion for the Hubbard model, Phys. Rev. B **37**, 9753 (1988).

[44] F. Kolley, S. Depenbrock, I. P. McCulloch, U. Schollwöck, and V. Alba, Phase diagram of the $J_1 - J_2$ Heisenberg model on the kagome lattice, Phys. Rev. B **91**, 104418 (2015).

[45] N. Morales-Durán, N. C. Hu, P. Potasz, and A. H. MacDonald, Nonlocal Interactions in Moiré Hubbard Systems, Phys. Rev. Lett. **128**, 217202 (2022).

[46] N. Morales-Durán, P. Potasz, and A. H. MacDonald, Magnetism and Quantum Melting in Moiré-Material Wigner Crystals, arXiv:2210.15168.

[47] M. Takahashi, Half-filled Hubbard model at low temperature, J. Phys. C: Solid State Phys. **10**, 1289 (1977).

[48] H. Pan, F. Wu, and S. Das Sarma, Band topology, Hubbard model, Heisenberg model, and Dzyaloshinskii-Moriya interaction in twisted bilayer WSe_2, Phys. Rev. Res. **2**, 033087 (2020).

[49] J. Zang, J. Wang, J. Cano, and A. J. Millis, Hartree-Fock study of the moiré Hubbard model for twisted bilayer transition metal dichalcogenides, Phys. Rev. B **104**, 075150 (2021).

[50] A. Wietek, J. Wang, J. Zang, J. Cano, A. Georges, and A. Millis, Tunable stripe order and weak superconductivity in the moiré Hubbard model, Phys. Rev. Res. **4**, 043048 (2022).

[51] S.-S. Gong, W. Zhu, L. Balents, and D. N. Sheng, Global phase diagram of competing ordered and quantum spin-liquid phases on the kagome lattice, Phys. Rev. B **91**, 075112 (2015).

[52] Y.-C. He, D. N. Sheng, and Y. Chen, Chiral Spin Liquid in a Frustrated Anisotropic Kagome Heisenberg Model, Phys. Rev. Lett. **112**, 137202 (2014).

[53] S.-S. Gong, W. Zhu, and D. N. Sheng, Emergent chiral spin liquid: Fractional quantum Hall effect in a kagome Heisenberg model, Sci. Rep. **4**, 6317 (2014).

[54] Y.-C. He and Y. Chen, Distinct Spin Liquids and Their Transitions in Spin-1/2 XXZ Kagome Antiferromagnets, Phys. Rev. Lett. **114**, 037201 (2015).

[55] A. Wietek, A. Sterdyniak, and A. M. Läuchli, Nature of chiral spin liquids on the kagome lattice, Phys. Rev. B **92**, 125122 (2015).

[56] A. B. Harris, C. Kallin, and A. J. Berlinsky, Possible néel orderings of the kagomé antiferromagnet, Phys. Rev. B **45**, 2899 (1992).

[57] R. R. P. Singh and D. A. Huse, Three-Sublattice Order in Triangular- and Kagomé-Lattice Spin-Half Antiferromagnets, Phys. Rev. Lett. **68**, 1766 (1992).

[58] S. Sachdev, Kagome′- and triangular-lattice Heisenberg antiferromagnets: Ordering from quantum fluctuations and quantum-disordered ground states with unconfined bosonic spinons, Phys. Rev. B **45**, 12377 (1992).

[59] L. Messio, C. Lhuillier, and G. Misguich, Lattice symmetries and regular magnetic orders in classical frustrated antiferromagnets, Phys. Rev. B **83**, 184401 (2011).

[60] C. Zeng and V. Elser, Numerical studies of antiferromagnetism on a Kagomé net, Phys. Rev. B **42**, 8436 (1990).

[61] X. G. Wen, Gapless boundary excitations in the quantum Hall states and in the chiral spin states, Phys. Rev. B **43**, 11025 (1991).

[62] H. Li and F. D. M. Haldane, Entanglement Spectrum as a Generalization of Entanglement Entropy: Identification of Topological Order in Non-Abelian Fractional Quantum Hall Effect States, Phys. Rev. Lett. **101**, 010504 (2008).

[63] X.-L. Qi, H. Katsura, and A. W. W. Ludwig, General Relationship between the Entanglement Spectrum and the Edge State Spectrum of Topological Quantum States, Phys. Rev. Lett. **108**, 196402 (2012).

[64] R. R. P. Singh and D. A. Huse, Ground state of the spin-1/2 kagome-lattice Heisenberg antiferromagnet, Phys. Rev. B **76**, 180407(R) (2007).

[65] H.-C. Jiang, Z. Wang, and L. Balents, Identifying topological order by entanglement entropy, Nat. Phys. **8**, 902 (2012).

[66] J.-W. Mei, J.-Y. Chen, H. He, and X.-G. Wen, Gapped spin liquid with $\mathbb{Z}_2$ topological order for the kagome Heisenberg model, Phys. Rev. B **95**, 235107 (2017).

[67] H. J. Changlani, D. Kochkov, K. Kumar, B. K. Clark, and E. Fradkin, Macroscopically Degenerate Exactly Solvable Point in the Spin-1/2 Kagome Quantum Antiferromagnet, Phys. Rev. Lett. **120**, 117202 (2018).

[68] S. Jiang, P. Kim, J. H. Han, and Y. Ran, Competing spin liquid phases in the $s = \frac{1}{2}$ Heisenberg model on the kagome lattice, SciPost Phys. **7**, 006 (2019).

[69] A. Wietek and A. M. Läuchli, Valence bond solid and possible deconfined quantum criticality in an extended kagome lattice Heisenberg antiferromagnet, Phys. Rev. B **102**, 020411(R) (2020).

[70] A. G. Salvador, C. Kuhlenkamp, L. Ciorciaro, M. Knap, and A. İmamoğlu, Optical Signatures of Periodic Magnetization: The Moiré Zeeman Effect, Phys. Rev. Lett. **128**, 237401 (2022).

[71] O. Kazakova, R. Puttock, C. Barton, H. Corte-León, M. Jaafar, V. Neu, and A. Asenjo, Frontiers of magnetic force microscopy, J. Appl. Phys. **125**, 060901 (2019).

[72] R. Wiesendanger, Spin mapping at the nanoscale and atomic scale, Rev. Mod. Phys. **81**, 1495 (2009).

[73] S. Chatterjee, J. F. Rodriguez-Nieva, and E. Demler, Diagnosing phases of magnetic insulators via noise magnetometry with spin qubits, Phys. Rev. B **99**, 104425 (2019).

[74] D. Xiao, G.-B. Liu, W. Feng, X. Xu, and W. Yao, Coupled Spin and Valley Physics in Monolayers of MoS_2 and Other Group-VI Dichalcogenides, Phys. Rev. Lett. **108**, 196802 (2012).

[75] K. F. Mak, K. He, J. Shan, and T. F. Heinz, Control of valley polarization in monolayer MoS_2 by optical helicity, Nat. Nanotechnol. **7**, 494 (2012).

[76] S. Banerjee, W. Zhu, and S.-Z. Lin, Electromagnetic signatures of chiral quantum spin liquid, arXiv:2304.08635.

[77] M. Claassen, L. Xian, D. M. Kennes, and A. Rubio, Ultrastrong spin–orbit coupling and topological moiré engineering in twisted ZrS_2 bilayers, Nat. Commun. **13**, 4915 (2022).

[78] A. P. Reddy, T. Devakul, and L. Fu, Moiré alchemy: Artificial atoms, Wigner molecules, and emergent Kagome lattice, arXiv:2301.00799.

[79] J. Motruk, D. Rossi, and L. Rademaker, Kagome chiral spin liquid in transition metal dichalcogenide moiré bilayers [Data set], Université de Genève, Yareta, https://doi.org/10.26037/yareta:y635nolybbdfjjvwovjwm3dnmm.

[80] J. Hauschild and F. Pollmann, Efficient numerical simulations with Tensor Networks: Tensor Network Python (TeNPy), SciPost Phys. Lect. Notes, 5 (2018); code available from https://github.com/tenpy/tenpy.